# Microstructural and mechanical behavior of highly deformed Al–Sn alloys

*O. Hernández, G. Gonzalez**

*Instituto de Investigaciones en Materiales, Universidad Nacional Autónoma de México, Ciudad Universitaria, A.P. 70-360, 04510 México D.F.*

ARTICLE DATA

*Article history:*
Received 28 August 2006
Received in revised form
21 March 2007
Accepted 23 March 2007

*Keywords:*
Mechanical properties
Composites
Rolling
In situ composites
DMMCs

ABSTRACT

Tensile strength and microstructural evolution were evaluated for the deformation processed metal–metal composites of Al–*X* vol.% Sn, where *X*=3.96, 16.32, 20. Samples were prepared by casting, and deformed by cold rolling. The material was characterized by scanning electron microscopy and focused ion beam. In the case of larger true strains $\eta>5$, the composite presents an unexpected increase in tensile strength compared to the rule of mixtures. During cold rolling, the Sn phase developed a lamellar morphology and geometrical aspects, as its separation and thickness were correlated with the tensile strength of the composite. A study of the peak broadening was made by using X-ray diffraction, in order to measure the microstrains inside the composite, and correlate them with the macroscopic strength.



## 1. Introduction

Deformation processed metal–metal composites (DMMCs) are materials where an oriented filamentary microstructure is created through severe plastic deformation. Because the filamentary microstructure is formed within the specimen as it is deformed, these materials are often called "in situ composites". In general, DMMCs are produced by this sequence: starting billets are prepared with powder metallurgy or castings methods, then they are formed by axisymmetric deformation such as extrusion, wire drawing or rolling.

Throughout the study of DMMCs, the following observations have been made:

(a) A severe deformation of a mixture of two immiscible and ductile phases can produce sheet or wire materials with unexpected high tensile strengths [1–5], and these can be significantly in excess of values predicted by the rule of mixtures.

(b) As a result of extensive cold working, the dislocation density appears to continuously increase while the second phase size decreases, developing a final microstructure in the micron scale.

(c) Tensile strengths resulting from cold working are dependent on the crystal symmetry of the two phases, being greater for fcc–bcc (Cu–Fe, Cu–Cr [6], Cu–Nb [1]) combinations than for fcc–fcc (Ag–Ni [6], Ag–Cu [7]) combinations [2].

(d) Tensile strengths of DMMCs deformed up to about 99.5%, have been shown to correlate with filament spacing, leading to a Hall–Petch relationship [8,9], regardless of whether the composites were of the fcc–bcc or fcc–fcc type [10].

The greater strengthening which results in the fcc–bcc composites, has been attributed to the bcc filaments which develop a convoluted ribbon shape, as a result of the {110} fiber texture produced during cold working [11]. In the nineties,

* *Corresponding author*. Tel.: +52 5556224642.
*E-mail address:* joseggr@servidor.unam.mx (G. Gonzalez).

1044-5803/$ – see front matter © 2007 Elsevier Inc. All rights reserved.
doi:10.1016/j.matchar.2007.03.012

some studies with hcp Metals (Ti–Y [12], Mg–Ti [13], Al–Mg [14]) were made. For the fcc–hcp combination, in particular in Al–Ti and Al–Mg, the microstructures are quite similar to that of fcc–bcc DMMCs [15]. Nowadays, there is not much research work with DMMCs whose second phase is not fcc, bcc or hcp. Rusell et al. [15] studied a DMMC with a fcc matrix containing a body centered tetragonal (bct) second phase Sn (Al–20 vol.% Sn). This composite was deformed by extrusion to $\eta$=7.41 ($\eta$ represents the true strain deformation). The correlation in Al–20 vol.% Sn between the tensile strength and $\eta$ led to an exponential growth [15], and its resistance increased from 150 MPa with $\eta$=3 to 290 MPa with $\eta$=7.41, which means an increment of 100%.

In order to complete the Russell study, this work investigated the Al–X vol.% Sn system, where X=3.96, 16.32, 20 deformed by rolling. The role of Sn content on tensile strength was explored, as well as the effect on mechanical properties due to the morphology of Sn developed rolling. This work compares the effects of this morphology with the convoluted ribbon shape obtained by extrusion and correlates the tensile strength with the second phase spacing to see if the fcc–bct combination leads to a Hall–Petch relationship. The extensive deformation of DMMCs results in two important effects: one is work hardening due to the increase of the dislocation density; and the other, the interaction of the dislocations with the filaments boundaries. In this way, the present study tried to evaluate qualitatively, the evolution of microstrain at different levels of $\eta$ by X-ray techniques and the Rietveld method.

## 2. Experimental Procedures

Ingots of Al–X vol.% Sn where X=3.96, 16.32, 20.00 were prepared in an induction furnace in a graphite crucible. Al–99.6% and Sn of commercial purity were used as starting materials. The casting procedure consisted in heating the aluminum until a liquid state was reached, and then little pieces of tin were blended within the aluminum. All the processes were conducted under an argon atmosphere. Ingots were rolled at room temperature (300 K) with a starting height

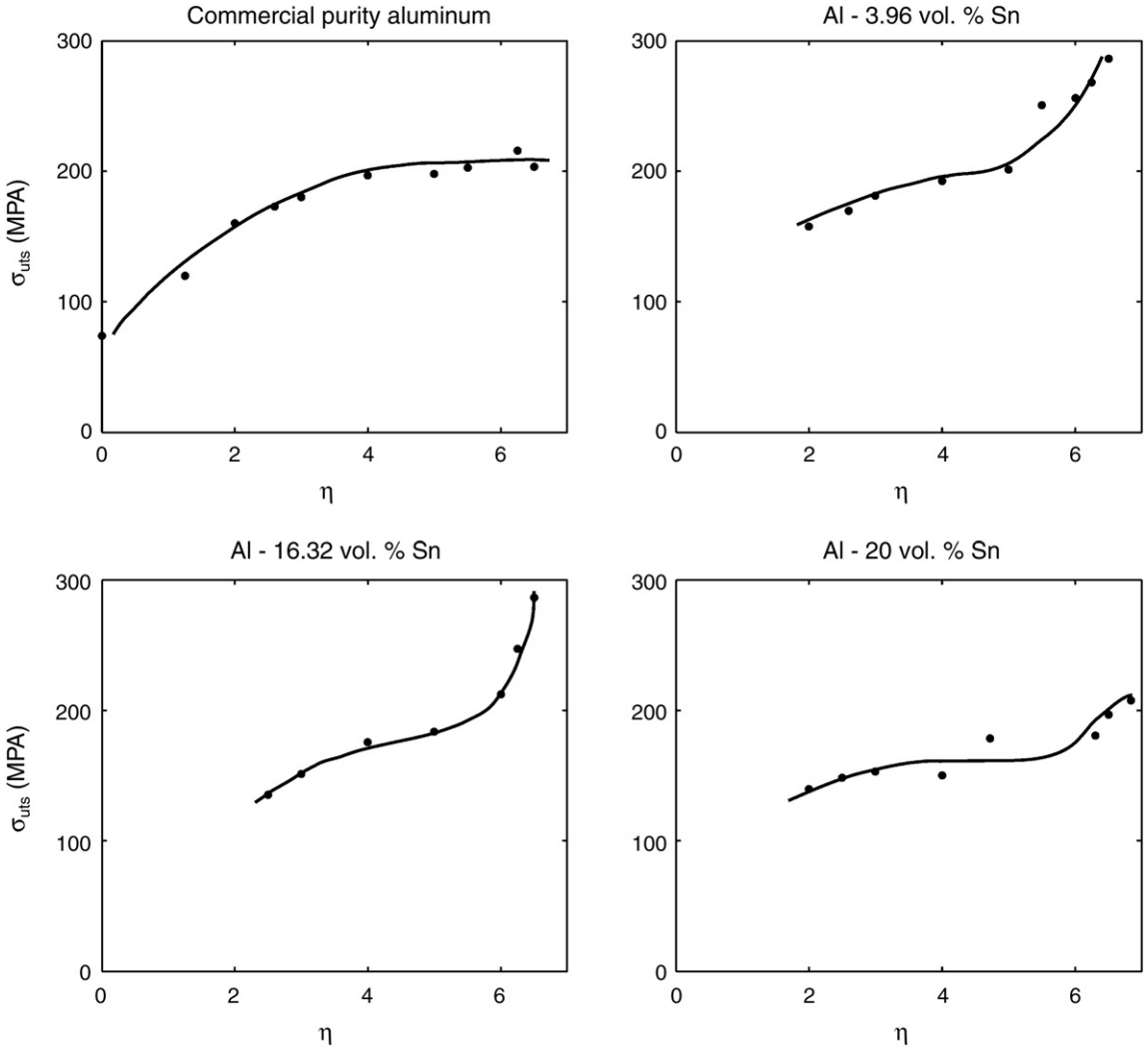


**Fig. 1 – Effect of the deformation true strain η on tensile strength $\sigma_{uts}$ for Al–X vol.% Sn where X=3.96, 16.32, 20 and aluminum (>99.6% purity).**

of 62 mm and a reduction of 1 mm per step, the tangential velocity of the rolls was 10 m/min. Metallographic and tensile specimens were cut at true strain deformations of $\eta$=2.5, 3, 4, 5, 6, 6.25, and 6.5. For sheet material, the true strain deformation is given by $\eta=\ln(t_0/t_f)$, where $t_0$ and $t_f$ are the initial and final thicknesses, respectively.

The microstructural study was performed on a Cambridge–LEICA 440 Scanning Electron Microscope. X-ray measurements were made with a D8 Advance BRUKER Diffractometer. Focused Ion Beam images were made with a PHILIPS FEI 200 in order to make a micro cavity in transverse sections and analyze the Sn second phase morphology.

In order to analyze the evolution of the second phase microstructure as a function of $\eta$, SEM images were analyzed for the composition 3.96 vol.% Sn starting at deformation levels of $\eta$=4. This was done in order to have a sufficient separation between the Sn phase and obtain more accurate results. The spacing between the Sn phase was measured using the mean linear intercept method. In order to track the effect of the dislocation density on the microstrains developed inside the aluminum, a study of peak broadening was performed.

Tensile tests were conducted for all specimens according to the standard ASTM E8M procedure at room temperature, with a deformation rate of 1.0 mm/min, and at least three specimens were tested, each at the true strain deformation previously mentioned.

## 3. Results and Discussion

### 3.1. *Mechanical Properties*

Fig. 1 shows a set of curves which correlates the ultimate tensile strength $\sigma_{uts}$ with the parameter $\eta$ for the Al–X vol.% Sn (X=3.96, 16.32, 20) and commercial pure aluminum. The latter presents a strength saturation for deformation values higher than 5; while the former, specifically for the compositions 3.96 and 16.32 vol.% Sn, presents an unexpected increase in $\sigma_{uts}$ at the same point. The strength saturation of aluminum at large strains, is the result of the material's dynamic recovery, given that at a certain deformation level there is equilibrium between the creation and annihilation of dislocations: the dislocation density is kept constant and no further work hardening is presented. With regard to the composition Al–20 vol.% Sn, Russell et al. [15] reported a strength of 288 MPa with $\eta$=7.41 when the composite is extruded. Fig. 1 shows that for this composition, the composite does not present a significant increase in $\sigma_{uts}$ as it is deformed, and the values obtained are less in comparison to the extruded composite. Nevertheless, if the strengths for the compositions 3.96 and 16.32 vol.% Sn are compared to Russell et al. results, similar strengths are observed.

To make a comparison between two different deformation processes, in this case rolling and extrusion, an effective deformation strain must be used. For rolled sheet, this effective strain is given by $\eta_e=2/\sqrt{3}\eta$ [16]. Thus, in the case of rolling, for $\eta$=6.5 which correlates to a strength of 286 MPa, the effective strain is calculated by

$$\eta_e = 2/\sqrt{3} \times 6.5 = 7.5 \quad (1)$$

That deformation corresponds to a strength of 288 MPa according to Russell's results [15], this difference is only about of 0.7%. This result shows an equivalence in the strengths obtained between the microstructures produced by two deformation processes if the adequate composition is chosen. The microstructure produced by rolling is different from the one produced by extrusion, as shown in the microstructural characterization section.

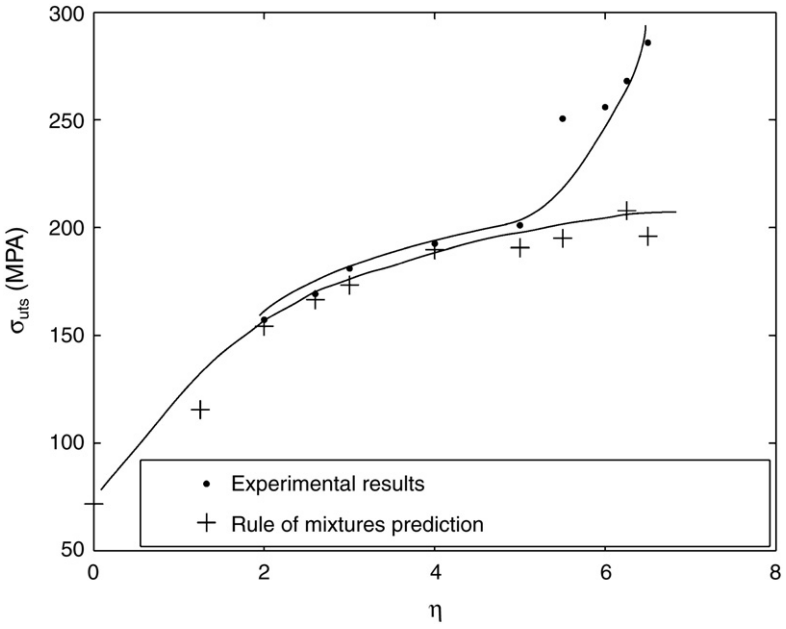


**Fig. 2 – Comparison between the experimental results obtained for Al–3.96 vol.% Sn and the rule of mixtures prediction.**

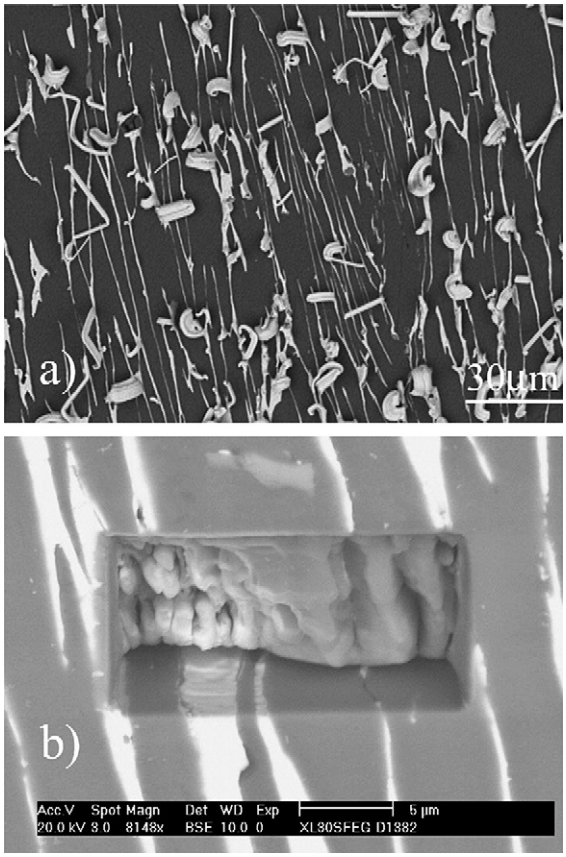


**Fig. 3 – (a) SEM and (b) FIB images showing the microstructure in transverse section of the Al–3.96 vol.% Sn rolled at $\eta$=2.5. Aluminum matrix is shown as dark gray; tin is shown in white.**

The strengths obtained in the composite exceed the values predicted by the rule of mixtures (ROM). Fig. 2 shows a strength comparison between the 3.96 vol.% Sn composition and the ROM estimated values. The ROM expression used to calculate the composite's strength was:

$$\sigma_{c\,uts} = \sigma_{f\,uts} V_f + \sigma_m\ V_m \qquad (2)$$

where $\sigma_{c\,uts}$ and $\sigma_{f\,uts}$ are the ultimate tensile strengths of the composite and the second phase, respectively, and $V_f$ and $V_m$ the volume fractions. In this case, $\sigma_m$ was chosen as the ultimate tensile strength of the cold worked matrix to obtain an upper limit of the composite strength. Tin should not present strain hardening because its recrystallization temperature is below that of room temperature. Accordingly, $\sigma_f$ was considered constant and equal to 14 MPa, which is the tensile strength of Sn. As shown in the figure, the composite presents a deviation from ROM for values $\eta$>5 which corresponds to the same break point presented in the curves $\sigma_{uts}$–$\eta$.

### 3.2. *Microstructural Characterization*

Microstructures of Al–16.32 vol.% Sn were obtained from transverse sections at two deformation levels. Furthermore, in order to observe some 3D morphology features, we completed the SEM images with a FIB picture, in which the depth is revealed by a cavity formed just below the Sn phase. At $\eta$=2.5, Fig. 3 shows that Sn morphology exhibits a relatively curled ribbons microstructure parallel to the rolling plane. At $\eta$=6, Fig. 4 show that Sn curled ribbons change toward a lamellar or stripe microstructure. The thickness and separation of Sn stripes became smaller while the deformation true strain increased. Fig. 5 shows this behavior for the composition 3.96 vol.% Sn.

The correlation between $\sigma_{uts}$ and the thickness of Sn phase is presented in Fig. 6. As the figure shows, there is an increase of 50% in tensile strength while the thickness decreases in a ratio of 1:3; this leads us to think that the second-phase thickness is an important factor in the overall resistance of the composite.

In Fig. 7, the data for $\sigma_{uts}$ was plotted against $d^{-1/2}$, where $d$ is the mean separation between the Sn phase for deformation true strains $\eta$=4, 5, 6, 6.25 and 6.5. This figure shows a good correlation with the Hall–Petch relationship, for a composite with a combination fcc–bct. In this way the composite strengthening can be explained by a Hall–Petch barrier model, where the Sn plates, at certain spacing and thickness conditions, act as effective barriers to dislocation motion. This correlation had been observed in other composites such as Cu–Nb [4], (Cu–Cr, Cu–Fe, Ag–Ni) [10].

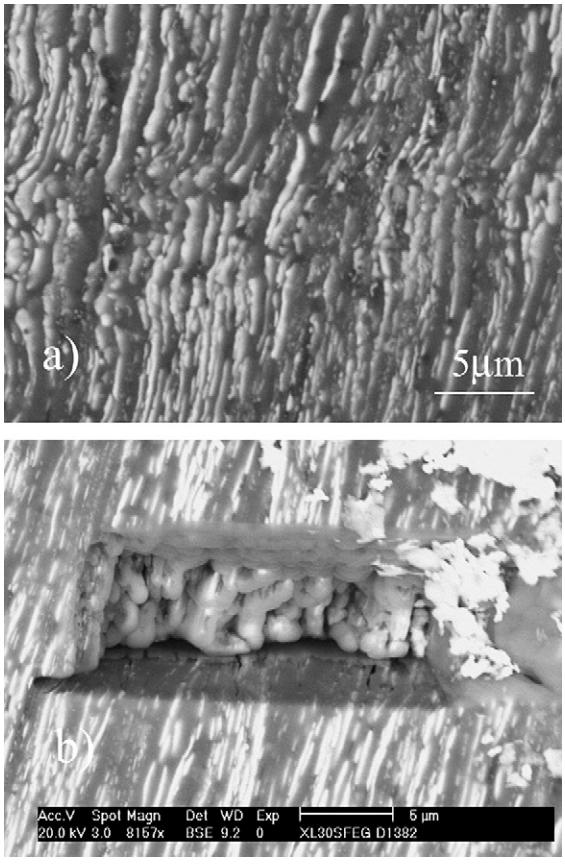


**Fig. 4 – (a) SEM and (b) FIB images showing the microstructure in transverse section of the Al–16.32 vol.% Sn rolled at $\eta$=6. Aluminum matrix is shown as dark gray; tin is shown in white.**

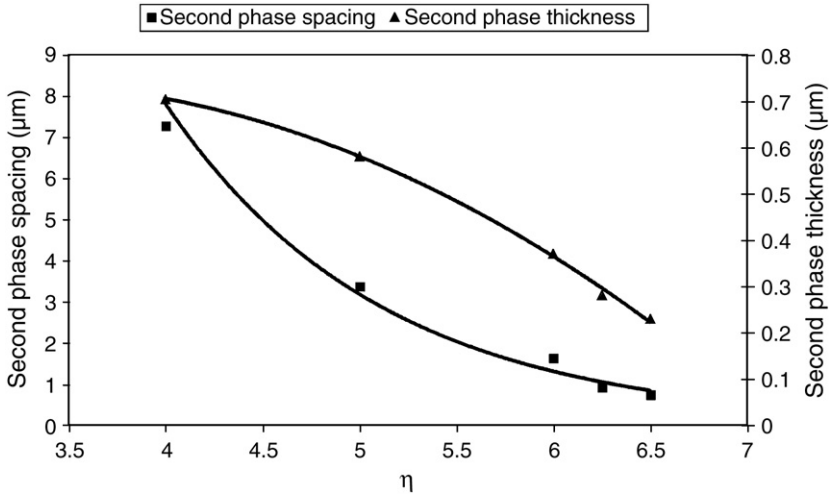


**Fig. 5 – Thickness and separation of Sn phase at different deformation true strains for Al–3.96 vol.% Sn.**

Up to this point, the present work has shown the relationship between the ultimate tensile strength and diverse parameters as are true strain deformation, thickness and second phase spacing. With respect to the break point presented in the curve $\sigma_{uts}$–$\eta$, this work attempts to evaluate microstructural aspects as microstrains, which reflects the evolution of dislocation density. This study was carried out by analyzing the diffraction peak broadening by X-ray techniques and taking advantage of the refinement capabilities of the Rietveld Method. Specimens for the composition 16.32 vol.% Sn were analyzed at deformations true strains $\eta$=0, 2.5, 3, 4, 5, 6 and 6.5. Fig. 8 shows the Rietveld refinement for the composition 16.32 vol.% Sn with $\eta$=2.5. Table 1 shows the fit parameters, obtained for the remaining $\eta$ values.

After refinements were done, aluminum integral breadths samples were taken from a microstructural file. Integral breadths of every reflection were then substituted in the maximum strain formula (which is derived from the Stokes–Wilson apparent strain equation $\eta=\beta\cot\theta$ [17]), and an average of '*Max. Strains*' was calculated:

$$\text{Max.Strain} = e = \eta/4 \;=\; \beta^{*}d/2 \tag{3}$$

$\beta$ is the integral breadth of the intrinsic profile at a certain reflection, $\beta^{*}=\beta\cos\theta/\lambda$, and $d$ is the interplanar distance.

Fig. 9 presents this result showing the evolution of maximum strain versus $\eta$ for Al–16.32 vol.% Sn. As in the curves of $\sigma_{uts}$–$\eta$, an undergo and pronounced increase of around $\eta$=5 is also presented, but unlike Fig. 1, it shows a decrease for $\eta$>5.5. It seems that there is a correlation between the microstrains and the strength up to $\eta$=5. It is thought that microstrains could have an influence on the overall composite strength, in

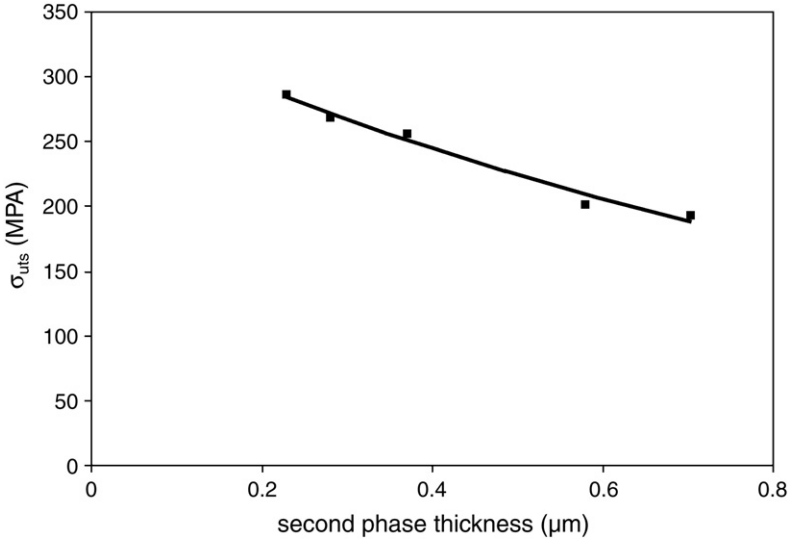


**Fig. 6 – Effect of Sn thickness on the tensile strength of the composite for Al–3.96 vol.% Sn.**

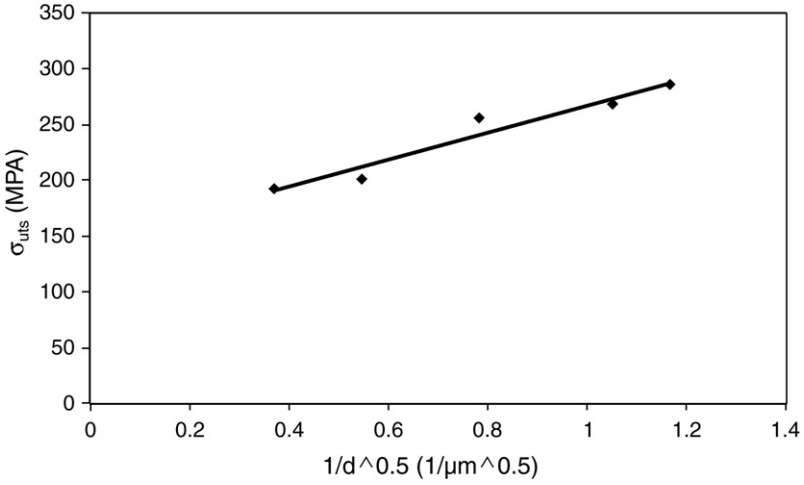


**Fig. 7 – Ultimate tensile strength dependence on the *d* spacing for Sn phase for Al–3.96 vol.% Sn.**

view of the fact that they are a part of the many microstructural conditions mentioned above, which apparently work together to produce this unexpected behavior.

## 4. Conclusions

An increment of 41% in $\sigma_{uts}$ is attained in the Al–X vol.% Sn ($X$=3.96, 16.32) at $\eta$=6.5, compared with commercial purity aluminum at the same level of true strain deformation. A critical true strain deformation point has been found at $\eta \geq 5$ where the thickness, the Sn phase spacing and the microstrain field combine to increase the $\sigma_{uts}$ in an unexpected way. For values below this critical point, the ultimate tensile strength follows a typical rule of mixtures relation. When the Al–Sn composite is rolled, the Sn phase adopts a 'lamellar microstructure' parallel to the rolling plane. A convoluted ribbon-shaped morphology also shows to be effective at hindering

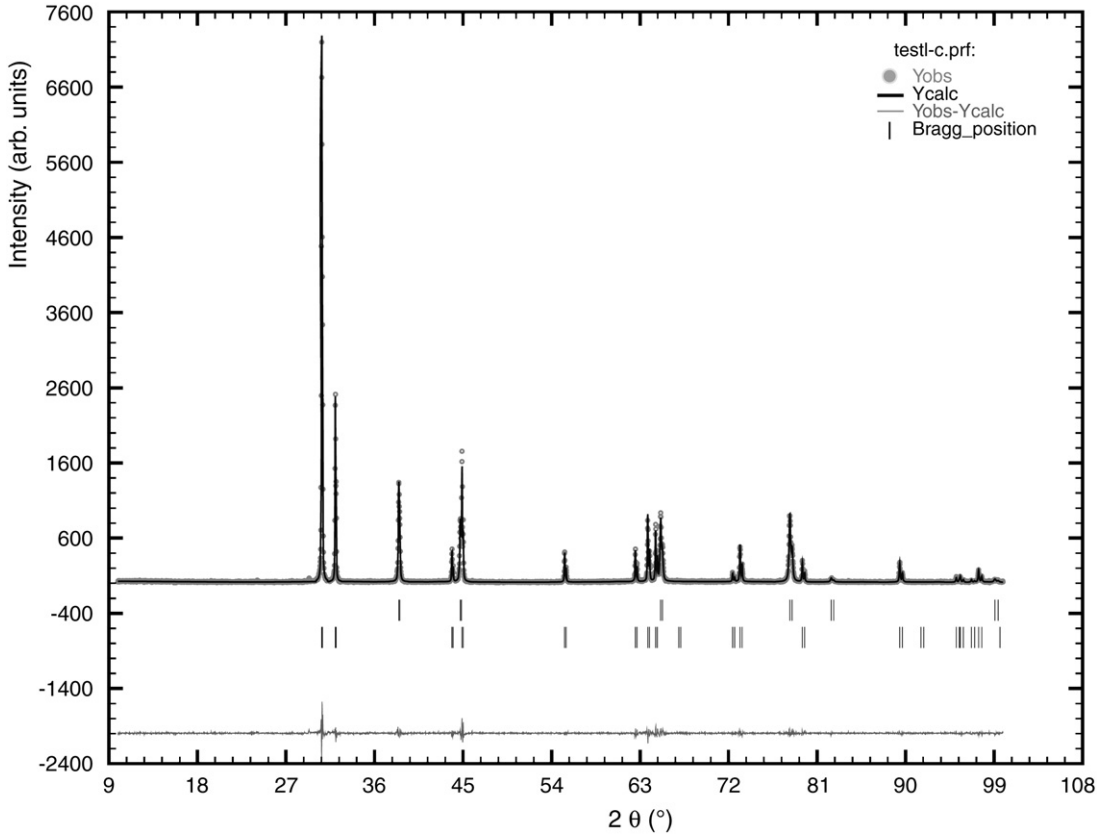


**Fig. 8 – Rietveld refinement for Al–16.32 vol.% Sn and η=2.5.**

**Table 1 – Rietveld refinement parameters for Al–16.32 vol. % Sn at different values of η**

| η | $R_f$ | $R_{wp}$ | $R_e$ | $\chi^2$ |
|---|---|---|---|---|
| 0 | 1.807 | 14.1 | 9.07 | 2.41 |
| 2.5 | 4.151 | 22.6 | 16.87 | 1.8 |
| 3 | 1.693 | 28.9 | 17.21 | 2.82 |
| 4 | 2.491 | 23.1 | 16.76 | 1.9 |
| 5 | 2.771 | 25.2 | 15.80 | 2.55 |
| 6 | 1.919 | 22.5 | 13.58 | 2.7 |
| 6.5 | 1.329 | 23.1 | 18.96 | 1.48 |

$$R_f = 100 \sum_{i=1}^{i=n} |I_i^{obs^{1/2}} - I_i^{calc^{1/2}}| / \sum_{i=1}^{i=n} I_i^{obs^{1/2}}$$

$\chi^2$ (Goodness of fit) = $(R_{wp}/R_e)^2$
where:

$$R_{wp} = 100\left(\sum_{i=1}^{i=n} w_i \left(y_i^{obs} - y_i^{calc}\right)^2 / \sum_{i=1}^{i=n} w_i y_i^{obs^2}\right)^{1/2}$$

$$R_e = 100\left[(N - P + C) / \left(\sum_{i=1}^{i=n} w_i y_i^{obs^2}\right)\right]^{1/2}$$

dislocation motion. As the Al–Sn composite is deformed, the thickness and the space between the second phase decrease in a non linear way with a different profile in both cases. There is a 'quasi linear' correlation between the second phase thickness and the ultimate tensile strength, attaining the highest strength with a mean thickness of 0.2 μm. The strengthening of the composite follows a Hall–Petch relationship. This proves that this correlation can be successfully adapted to a DMMC which involves cells fcc–bct.

Further work is in progress in order to establish whether the dislocation configuration can be revealed by TEM observations, and we will continue experimenting with other similar DMMCs to verify if these conclusions can be generalized.

## Acknowledgements

The authors are grateful to L. Baños, J. Guzmán, G. Lara, A. Maciel, W. Saikaly and C. Walford for technical assistance, and to Dr. Francisco Cruz Gandarilla for many fruitful discussions. This work was supported by PAPIIT-UNAM ref IN106005 and CONACYT.

## REFERENCES

[1] Bevk J, Harbison JP, Bell JL. Anomalous increase in strength of *in situ* formed Cu–Nb multifilamentary composites. Appl Phys 1978;49(12):6031–8.
[2] Spitzig WA, Krotz PD. A comparison of the strength and microstructure of heavily cold-worked Cu–20% Nb composites formed by different melting procedures. Scr Metall 1987;21:1143–6.
[3] Spitzig WA, Pelton AR, Laabs FC. Characterization of the strength and microstructure of heavily cold worked Cu–Nb composites. Acta Metall 1987;35:2427–42.
[4] Trybus CL, Spitzig WA. Characterization of the strength and microstructural evolution of a heavily cold rolled Cu–20% Nb composite. Acta Metall 1989;37:1971–81.
[5] Verhoeven JD, Chumbley LS, Laabs FC, Spitzig WA. Measurement of filament spacing in deformation processed Cu–Nb alloys. Acta Metall Mater 1991;39:2825–34.
[6] Funkenbusch PD, Courtney TH. On the strength of heavily cold worked *in situ* composites. Acta Metall 1986;33:913–22.
[7] Bevk J, Sunder WA, Dublon G, Cohen DE. In: Lemkey FD, Cline HE, McLean M, editors. Mechanical properties of Cu-based composites with in situ formed ultrafine filaments, in in situ composites IV. New York: North Holland; 1982. p. 121–33.
[8] Hall EO. The deformation and ageing of mild steel: III. Discussion of results. Proc Phys Soc B 1951;64:747.
[9] Petch NJ. The cleavage strength of polycrystals. J Iron Steel Inst 1953;174:25.

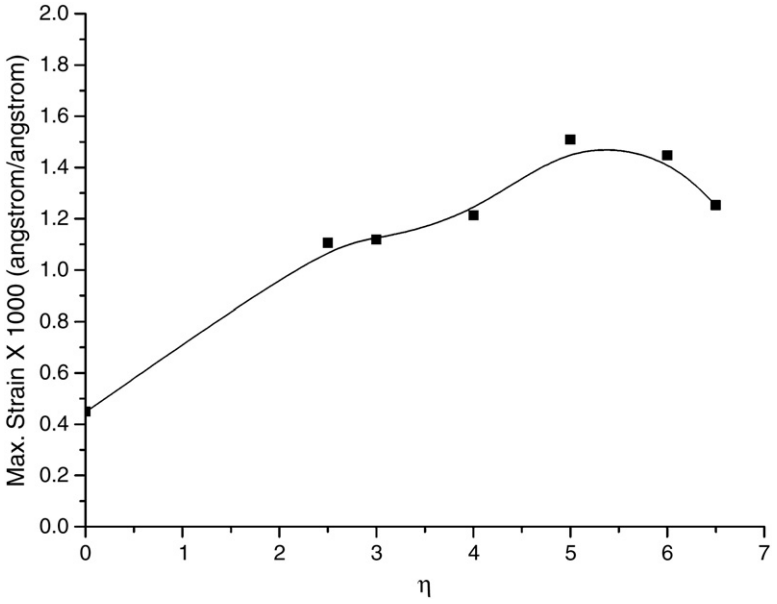


**Fig. 9 – Correlation between maximum strain versus η for Al–16.32 vol.% Sn.**

[10] Funkenbusch PD, Courtney TH, Kubisch DG. Fabricability of and microstructural development in cold worked metal matrix composites. Scr Metall 1984;18:1099–104.
[11] Frommeyer G, Wassermann G. Microstructure and anomalous mechanical properties of in situ-produced Ag/Cu composite wires. Acta Metall 1975;23:1353–60.
[12] Russell AM, Chumbley LS, Ellis TW, Laabs FC, Norris B, Donizetti GE. In situ strengthening of titanium with yttrium: texture analysis. J Mater Sci 1995;30:4249–62.
[13] Jensen JA, Rusell M, Ellis TW, Chumbley LS. HCP matrix in situ composites. In: Evans J, editor. Light metals. Warrendale, PA: TMS; 1995. p. 1367–74.
[14] Verhoeven JD, Spitzig WA, Schmidt FA, Trybus CL. Deformation processed copper–refractory metal composites. Mater Manuf Process 1989;4(2):197–209.
[15] Xu K, Rusell AM, Chumbley LS, Laabs FC. A deformation processed Al–20% Sn *in situ* composite. Scr Mater 2001;44:935–40.
[16] Johnson W, Mellor PB. Engineering plasticity. OH: Van Nostrand Reinhold; 1973. p. 109–10.
[17] Stokes AR, Wilson AJC. The diffraction of X rays by distorted crystal aggregates: I. Proc. Phys Soc Lond 1944;56:174.